The Role of Back-Reactions and Proton Uptake during the N → O Transition in Bacteriorhodopsin's Photocycle: A Kinetic Resonance Raman Study†

James B. Ames and Richard A. Mathies*
Department of Chemistry, University of California, Berkeley, California 94720
Received February 13, 1990; Revised Manuscript Received April 18, 1990

ABSTRACT: The kinetics of bacteriorhodopsin's photocycle have been analyzed at pH 5, 6, 7, 8, and 8.6 by using time-resolved resonance Raman spectroscopy. The concentrations of the various intermediates as a function of time were determined by following their resonance Raman intensities using 502-nm (L_{550}, N_{550}, BR_{568}), 458-nm (M_{412}), and 752-nm (O_{640}) excitation. The spectral contributions to the pump + probe data from each intermediate were quantitatively separated by least-squares decomposition. These relative concentrations were then converted to *absolute concentrations* by using a conservation of molecules constraint. This enabled the unambiguous refinement of a variety of kinetic models to find the simplest one that accurately describes the data. The kinetic data, including the biphasic decay of L_{550} and M_{412}, are best reproduced by a sequential scheme including back-reactions (BR → L ↔ M ↔ N → O → BR). In addition, the kinetics of the L ↔ M and N → O steps are found to be pH-dependent. Both the forward and reverse rate constants connecting L_{550} and M_{412} increase with pH, confirming earlier proposals of catalyzed Schiff base deprotonation at alkaline pH. Below pH 7, the N_{550} → O_{640} rate constant is independent of pH, but it decreases linearly with pH above 7. This indicates that the *protein* must pick up a proton during the N_{550} → O_{640} transition and that this process becomes rate determining above pH 7. There must, therefore, be an intermediate between N_{550} and O_{640} which we denote as N^{+}_{550}. A molecular graphics model is presented which incorporates these observations into a mechanism for proton pumping.

Bacteriorhodopsin (BR)[1] is an integral membrane protein found in the purple membrane of *Halobacterium halobium* which utilizes light energy to translocate protons across the bacterial cell membrane (Khorana, 1988; Stoeckenius & Bogomolni, 1982). Light absorption by the *all-trans*-retinal prosthetic group initiates a photochemical reaction called the photocycle (BR → J → K → L → M → N → O → BR). The initial photochemical step to produce J involves a femtosecond trans → cis torsional isomerization of the chromophore about the C_{13}=C_{14} bond (Mathies et al., 1988). The 13-cis Schiff base deprotonates during the formation of M_{412}, and this deprotonation is thought to be directly involved in the proton-pumping process. The Schiff base reprotonates with the formation of N_{550} (Fodor et al., 1988a), but reisomerization back to all-trans does not occur until O_{640} (Smith et al., 1983).

Models for the molecular mechanism of proton pumping generally involve photoisomerization and a pK_a change of the chromophore which causes proton release to the exterior. In the reset mechanism, the unprotonated chromophore in M_{412} probably accepts a proton from the cytoplasm before reisomerization (Kalisky et al., 1981; Schulten & Tavan, 1978). In more recent models this has been accomplished with a "reprotonation switch" which permits the 13-cis chromophore to transfer a proton to a residue connected to the exterior and subsequently pick up a proton from a cytoplasmic residue. Chromophore-based reprotonation switches which employ C_{14}–C_{15} bond rotation (Schulten & Tavan, 1978) or C=N bond inversion (Smith et al., 1986) before or after M_{412} appear unlikely because the chromophore configuration and conformation in L_{550}, M_{412}, and N_{550} are identical (Ames et al., 1989; Fodor et al., 1988a,b). This led us to propose the "C–T model" which employs a two-state protein conformational switch to regulate the connectivity of the Schiff base group (Fodor et al., 1988a).

Although the kinetics of the photocycle have been extensively studied, there is still disagreement over the kinetic scheme. The earliest photocycle model included the intermediates K_{590}, L_{550}, M_{412}, N_{550}, and O_{640} in a sequential scheme (Lozier et al., 1975). The elusive N intermediate has recently been better characterized[2] (Dancshazy et al., 1988; Drachev et al., 1986; Kouyama et al., 1988), and kinetic resonance Raman studies have indicated that N_{550} contains a 13-cis,15-anti protonated Schiff base chromophore and that it directly follows M_{412} in the photocycle (Fodor et al., 1988a). Alternatively, it has been argued that N_{550} arises from the photocycle of a second form of the pigment (Dancshazy et al., 1988; Diller & Stockburger, 1988). Photocycle schemes involving multiple forms of the pigment have also been proposed to account for the multiexponential kinetics of L_{550} and M_{412} (Alshuth & Stockburger, 1986; Hanamoto et al., 1984; Kouyama et al., 1988; Nakagawa et al., 1989). However, the multiexponential decay kinetics can also be consistent with a *single* sequential kinetic scheme if one includes back-reactions (Parodi et al., 1984). The issues in dispute are the origin of the pH-dependent biphasic kinetics of L_{550} and M_{412} and the kinetic origin of N_{550}.

Time-resolved resonance Raman spectroscopy is an effective method for probing the in situ structure and kinetics of the

† This research was supported by the National Institutes of Health (GM 27057) and the National Science Foundation (CHE 86-15093).
* To whom correspondence should be addressed.

[1] Abbreviations: BR, bacteriorhodopsin; HEPES, 4-(2-hydroxyethyl)-1-piperazineethanesulfonic acid; HOOP, hydrogen out of plane; PSB, protonated Schiff base.

[2] A green-absorbing intermediate that appears late in the photocycle has been variously identified as N_{550}, P, R_{350}, or L′. However, it appears that these species are identical. The intermediate identified as L′ (Diller & Stockburger, 1988) has a Raman spectrum that is identical with that of N_{550} (Fodor et al., 1988a); also the absorption spectrum reported for N_{550} (Kouyama et al., 1988) matches those of R_{350} and P (Dancshazy et al., 1988; Drachev et al., 1986). Therefore, we will call this species N_{550}.

0006-2960/90/0429-7181$02.50/0

transient photocycle intermediates because the Raman spectrum for each intermediate contains distinctive vibrational features (Mathies et al., 1987). In addition, selective enhancement of Raman scattering can be achieved by tuning the excitation wavelength into the absorption band of the desired intermediate. As a result, time-resolved resonance Raman spectroscopy can be used to probe the concentration of each intermediate as a function of time much more selectively than is possible with conventional transient absorption analyses. In this study, we have obtained kinetic Raman data on the various BR intermediates from pH 5 to 8.6. The results are modeled to reveal the simplest kinetic scheme that accurately describes the data. This provides an unambiguous characterization of the kinetic role of the N_{550} intermediate. Finally, the pH-dependent kinetics show that proton uptake by the protein occurs during the $N_{550} \rightarrow O_{640}$ transition.

Materials and Methods

Sample Preparation. Cultures of *H. halobium* (ET-1001) were grown, and the purple membrane was purified according to previously published procedures (Braiman & Mathies, 1980). Samples consisted of purple membrane fragments suspended in 3 M KCl, 0.5 M KNO_3 (internal intensity standard), and 10 mM HEPES or 10 mM borate (pH 8.6) at 30 °C. Addition of KNO_3 had no effect on the absorption or resonance Raman spectra of BR.

Time-Resolved Raman Spectroscopy. Transient Raman spectra were obtained by using a dual-beam flow apparatus (Mathies et al., 1987). The sample (1–2 OD/cm at 570 nm) was recirculated from a 20-mL reservoir through a 0.8-mm diameter glass capillary at 600 cm/s. The photocycle was initiated with a cylindrically focused 568- or 514.5-nm pump beam (0.8 mm height and 50 μm beam waist). The photoalteration parameter (Mathies et al., 1976) of the pump beam was ~1.2 assuming a maximum possible quantum yield of 0.6 (Schneider et al., 1989) and extinction coefficients of 63 000 M^{-1} cm^{-1} at 568 nm and 35 000 M^{-1} cm^{-1} at 514.5 nm. The depletion of BR_{568} and the formation of L_{550} were linear in pump power up to this level. Also, the spectrum of the L_{550} photointermediate under these conditions was identical with that obtained with a pump photoalteration of 0.1. The polarization of the pump beam was set to 54.7° relative to the probe beam polarization to eliminate photoselection artifacts. If the pump and probe beams had parallel polarizations, then the kinetics contained an artificial ~400-μs decay component for L_{550} and M_{412} and a similar recovery component for BR_{568} due to the reorientation of the purple membrane fragments. Raman scattering from M_{412} was excited with 30 mW at 457.9 nm; L_{550}, N_{550}, and BR_{568} were excited with 15 mW at 501.7 nm; and O_{640} was excited with 150 mW at 752.4 nm. In all cases, the probe beam was cylindrically focused (0.8 mm height and 50 μm beam waist) and the power was selected to produce a photoalteration parameter <0.1, assuming a photoreaction quantum yield of unity. To correct for changes in incident probe beam power and system alignment during the course of the experiment, all pump + probe and probe-only spectra were normalized to the intensity of the 1049-cm^{-1} nitrate standard. Also, about 5–10% of the chromophore bleached during the course of the experiment. To correct for this, probe-only spectra were taken at every delay time, and the integrated intensity for all lines between 1080 and 1700 cm^{-1} was used to correct for the loss in pigment.

Multichannel detection of the Raman scattering from L_{550}, M_{412}, N_{550}, and BR_{568} was accomplished by using a dry ice cooled intensified vidicon detector (PAR 1205A/1205D) coupled to a double spectrograph with 4–5-cm^{-1} resolution. O_{640} spectra were acquired with a scanning double-monochromator, photon-counting system using a 2-cm^{-1} step size, 2-s dwell time, and 4-cm^{-1} resolution. All spectra were corrected for the wavelength dependence of the spectrometer efficiency by using a standard lamp. Fluorescence backgrounds were removed by using a cubic spline fitting routine.

The different kinetic components in the pump + probe spectra were quantitatively separated by least-squares decomposition of the observed data using Raman basis spectra for L_{550}, M_{412}, N_{550}, O_{640}, and BR_{568}. The Raman basis spectra were obtained under conditions where each intermediate species was a major contributor to the pump + probe spectrum (see Figure 1). In each case, the specified fraction of the probe-only spectrum was subtracted from the pump + probe spectrum to minimize positive or negative peaks from the 1527-, 1201-, and 1214-cm^{-1} bands of BR_{568}.

The L_{550} Raman spectrum was obtained at the earliest measurable delay time of 20 μs at neutral pH. These conditions produce maximal L_{550} concentration (see below). The L_{550} spectrum has an ethylenic doublet at 1538 and 1550 cm^{-1} and fingerprint modes at 1191 and 1199 cm^{-1}. This spectrum is identical with those reported previously (Alshuth & Stockburger, 1986; Argade & Rothschild, 1983; Diller & Stockburger, 1988; Fodor et al., 1988b; Nakagawa et al., 1989; Terner et al., 1979).

The N_{550} Raman spectrum was obtained at 1 ms and neutral pH. Although the steady-state N_{550} concentration increases with pH, neutral pH conditions were chosen to ensure that the spectral decomposition was performed with the spectrum of the "neutral" form of N_{550}. It should be noted, however, that no evidence for a change in the spectrum of N_{550} was observed as a function of pH contrary to the suggestions of Chernavskii et al. (1989). The 1-ms delay time was chosen to give maximal N_{550} concentration at pH 7 (see below), which is in agreement with delay times used by Diller and Stockburger (1988). The N_{550} Raman spectrum in Figure 1 contains characteristic ethylenic lines at 1531 and 1548 cm^{-1}, two fingerprint lines at 1186 and 1202 cm^{-1}, and a methyl rock at 1006 cm^{-1}. These spectral features are in agreement with N_{550} spectra reported previously (Alshuth & Stockburger, 1986; Diller & Stockburger, 1988; Fodor et al., 1988a). It should also be noted that the L_{550} and N_{550} spectra have distinguishable ethylenic, fingerprint, and methyl rock modes which clearly indicate that these are different chemical species.

The M_{412} spectrum obtained at 200 μs (when the M_{412} concentration is maximal) is characterized by its distinctive 1566-cm^{-1} ethylenic mode, in agreement with M_{412} spectra reported previously (Alshuth & Stockburger, 1986; Ames et al., 1989; Aton et al., 1977; Braiman & Mathies, 1980; Deng et al., 1985; Nakagawa et al., 1989). The M_{412} ethylenic is so prominent in the pump + probe spectrum that the optimum subtraction parameter is unambiguous.

The O_{640} spectrum obtained at 2 ms delay and pH 7 is characterized by its 1508-cm^{-1} ethylenic mode, in agreement with O_{640} Raman spectra reported by Smith et al. (1983).

The Raman basis spectra were used to least squares decompose the kinetic pump + probe data in the spectral range 1080–1700 cm^{-1} and thereby extract the relative concentrations of L_{550}, M_{412}, N_{550}, O_{640}, and BR_{568} as a function of time. The spectral range in the decomposition analysis was limited to 1080–1700 cm^{-1} to avoid interference from the 1049-cm^{-1} nitrate band. The BR_{568} and M_{412} basis spectra (excited at 457.9 nm) were combined to simulate the kinetic pump + probe spectra excited at 457.9 nm. The M_{412} scattering is so strong with this probe wavelength that its kinetic amplitude

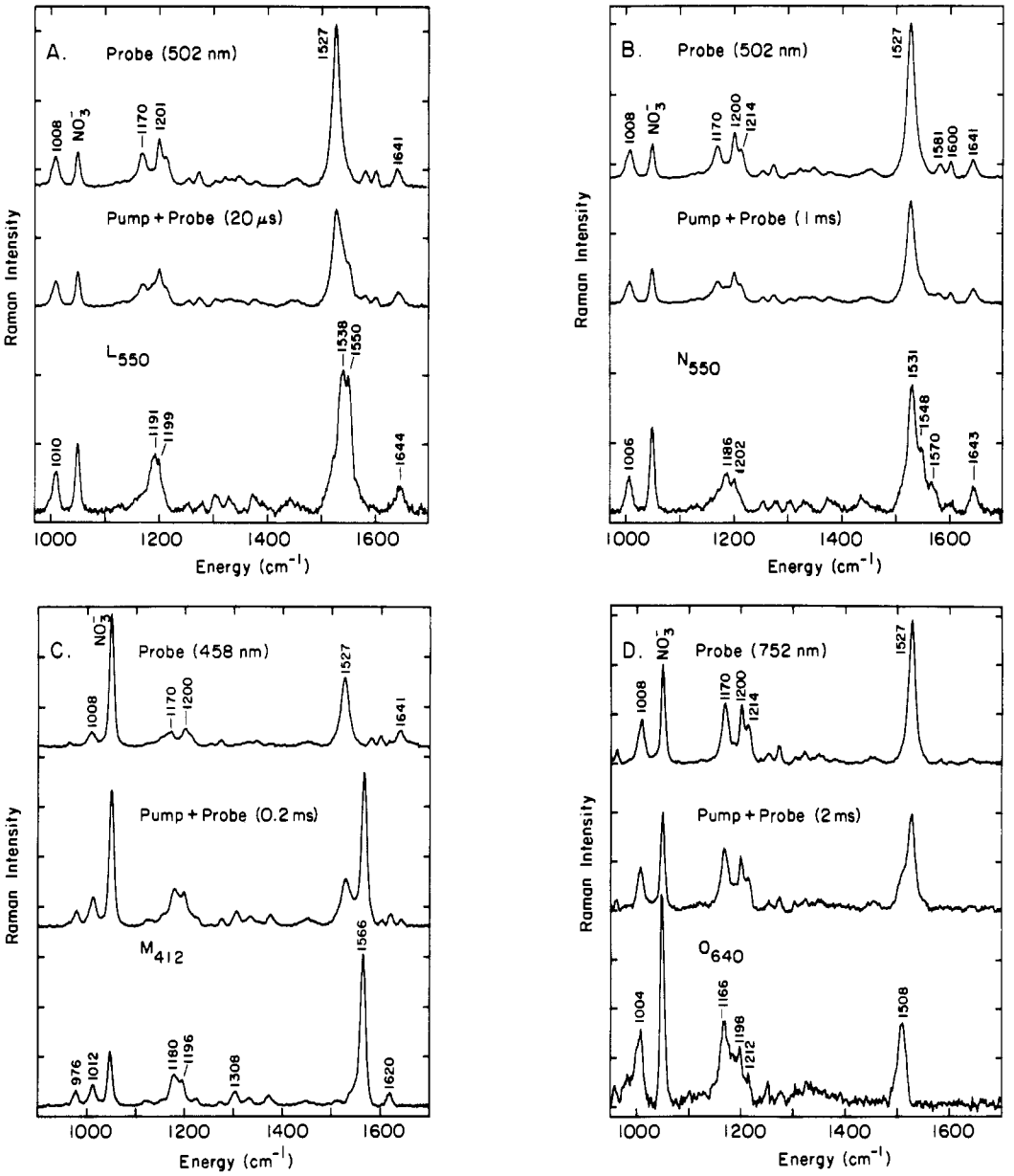

FIGURE 1: Time-resolved resonance Raman basis spectra for L_{550}, M_{412}, N_{550}, O_{640}, and BR_{568} at pH 7. (A) L_{550} spectrum obtained by subtracting 54% of the probe-only spectrum from the pump + probe spectrum; the L_{550} Raman spectrum was expanded 4-fold for display. (B) N_{550} spectrum obtained by subtracting 54% of the probe-only spectrum from the pump + probe spectrum; the N_{550} spectrum was expanded 5-fold. (C) M_{412} spectrum obtained by subtracting 54% of the probe-only spectrum from the pump + probe spectrum. (D) O_{640} spectrum obtained by subtracting 65% of the probe-only spectrum from the pump + probe spectrum; the O_{640} spectrum was expanded 6-fold. All probe-only and pump + probe spectra were normalized to the nitrate intensity before subtraction. The pump power was 140 mW at 568 nm for panels A–C and 250 mW at 514.5 nm for panel D. The delay times were determined by measuring the center-to-center distances between the two beams with a translation stage.

is not affected by the omission of L_{550} and N_{550} in the spectral decomposition. The L_{550}, N_{550}, and BR_{568} basis spectra (excited at 501.7 nm) were combined to simulate the pump + probe spectra excited at 501.7 nm.[3] Finally, BR_{568} and O_{640} basis spectra (obtained with 752.4-nm excitation) were used to simulate the pump + probe spectra excited at 752.4 nm. This analysis utilized a broad spectral region (1080–1700 cm^{-1}) instead of just the ethylenic region to permit a more constrained discrimination between L_{550} and N_{550}.

Determination of Absolute Concentrations. The least-squares decomposition coefficients determined above are proportional to the intermediates' concentration. Without further analysis, it is impossible to relate the relative concentration of one intermediate to that of another because they were obtained by using three different excitation wavelengths. To resolve this problem and obtain absolute concentrations for each kinetic species, we employ a conservation of molecules constraint which requires that the sum of the concentrations of all the intermediates at all times must be unity:

$$\{[L] + [M] + [N] + [O] + [BR]\}/[BR_o] = 1 \quad (1)$$

where BR_o is the overall pigment concentration. Since Raman intensity is proportional to concentration times the scattering cross section, σ, eq 1 becomes

$$[I_L(t)/\sigma_L + I_M(t)/\sigma_M + I_N(t)/\sigma_N + I_O(t)/\sigma_O + I_{BR}(t)/\sigma_{BR}]\sigma_{BR} = 1 \quad (2)$$

where $I_i(t)$ is the integrated Raman intensity for all lines in the fitting region from intermediate i at time t normalized to that of BR_{568} at $t = 0$ and σ_i is the integrated scattering cross

[3] The 501.7-nm spectra were used to determine the BR_{568} kinetics since the BR_{568} concentration is more accurately determined at this wavelength than at 752.4 or 457.9 nm.

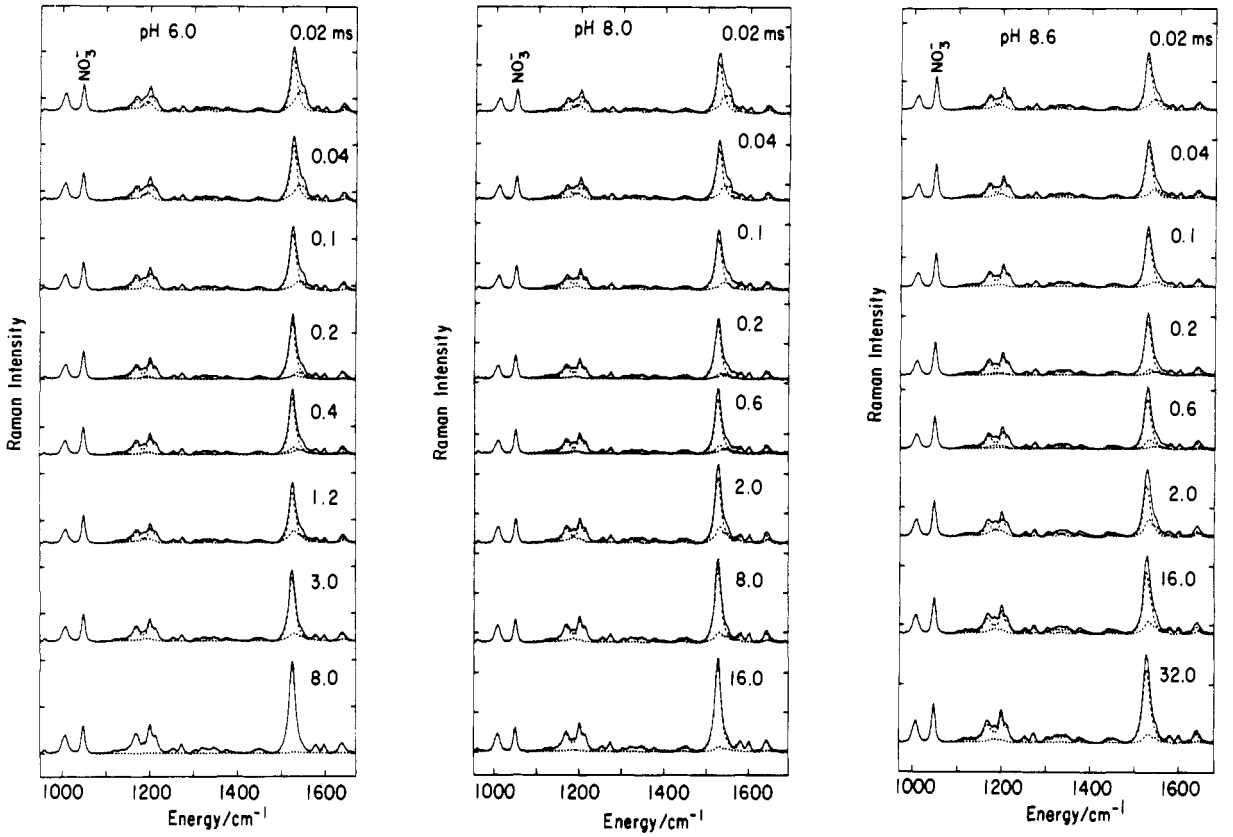

FIGURE 2: Kinetic pump + probe resonance Raman spectra of BR_{568}, L_{550}, and N_{550} at pH 6, 8, and 8.6 (probed at 501.7 nm). Spectra were normalized to the nitrate intensity and corrected for pigment bleaching as described under Materials and Methods. The dotted lines represent contributions from BR_{568}, L_{550}, and N_{550} determined from the least-squares fitting procedure.

section for intermediate *i*. The relative cross sections (σ_i/σ_{BR}) were constrained to be pH-independent and were least squares refined to preserve conservation of molecules at all times and pH's. Since we are fitting the 1080–1700-cm^{-1} region of the Raman spectrum, the refinement was performed with the total Raman intensity for all lines in this spectral region rather than just a single line. This was determined by mutliplying the least-squares fitting parameters by the integrated intensities of the bands in the basis spectra and then normalizing to the total intensity of the BR_{568} probe-only spectrum.

Kinetic Modeling. The concentration profiles of L_{550}, M_{412}, N_{550}, O_{640}, and BR_{568} were refined to a series of kinetic models. If the elementary steps of a kinetic scheme are first-order reactions, then we can write down a general set of differential equations to describe this process:

$$\dot{\mathbf{c}} = \mathbf{K}\cdot\mathbf{c} \tag{3}$$

where $\dot{\mathbf{c}}$ is a vector of the derivatives of the concentration of all the species with respect to time, **c** contains the concentrations as a function of time, and **K** is a matrix of microscopic rate constants. The type of kinetic scheme employed defines the **K** matrix (Cantor & Schimmel, 1980). The solution to this set of differential equations will be a set of linear combinations of decaying exponentials:

$$\mathbf{c} = \mathbf{A}\exp(-\mathbf{b}t) \tag{4}$$

Taking the derivative of **c** in eq 4 gives

$$\dot{\mathbf{c}} = -\mathbf{A}\cdot\mathbf{B}\exp(-\mathbf{b}t) \tag{5}$$

where **A** is a matrix of amplitudes and **B** is a diagonal matrix of apparent decay constants, **b**. Equating eqs 5 and 3 gives

$$\dot{\mathbf{c}} = -\mathbf{A}\cdot\mathbf{B}\exp(-\mathbf{b}t) = \mathbf{K}\cdot\mathbf{A}\exp(-\mathbf{b}t) \tag{6}$$

Therefore

$$\mathbf{A}\cdot\mathbf{B} = -\mathbf{K}\cdot\mathbf{A} \tag{7}$$

Equation 7 is an eigenvalue equation which determines the intrinsic component amplitudes **A** and decay constants **B**, given a set of microscopic rate constants **K**. **A** and **B** are then used in eq 4 to calculate the concentration profiles for L_{550}, M_{412}, N_{550}, O_{640}, and BR_{568}. A program was written to diagonalize the **K** matrix for an initial estimate of the rate constants. Then the rate constants were iterated according to a nonlinear least-squares procedure to minimize the deviation between the calculated and observed concentration profiles. This procedure finds an optimum set of rate constants for a given set of experimental concentration profiles and a given kinetic scheme.

Results

Spectral Decomposition of Kinetic Raman Data. Figures 2, 3, and 4 present a series of kinetic pump + probe spectra excited at 501.7, 457.9, and 752.4 nm, respectively, at pH 6, 8, and 8.6. Additional data at pH 5 and 7 are available as supplementary material; these data are qualitatively similar to the pH 6 data. In Figure 2, the 501.7-nm pump + probe spectra are decomposed into linear combinations of the BR_{568}, L_{550}, and N_{550} basis spectra indicated by the dotted lines. At early times (20–100 μs), the BR_{568} concentration remains constant as L_{550} decays. At intermediate times (0.1–0.8 ms), the decay of L_{550} continues but now we see some N_{550} appearing. At longer times (>1 ms) only BR_{568} and N_{550} contribute, and BR_{568} recovers with the decay of N_{550}. At higher pH, the L_{550} decay becomes faster while the N_{550} decay and BR_{568} rise become slower. In Figure 3 the 457.9-nm pump + probe spectra are decomposed into linear combinations of BR_{568} and M_{412} basis spectra. The rise and decay of M_{412} can be clearly seen in the raw data. As the pH increases, the M_{412} concentration rises faster and decays with a more pronounced slow component. In Figure 4 the 752.4-nm pump + probe spectra are decomposed into linear combinations of BR_{568} and

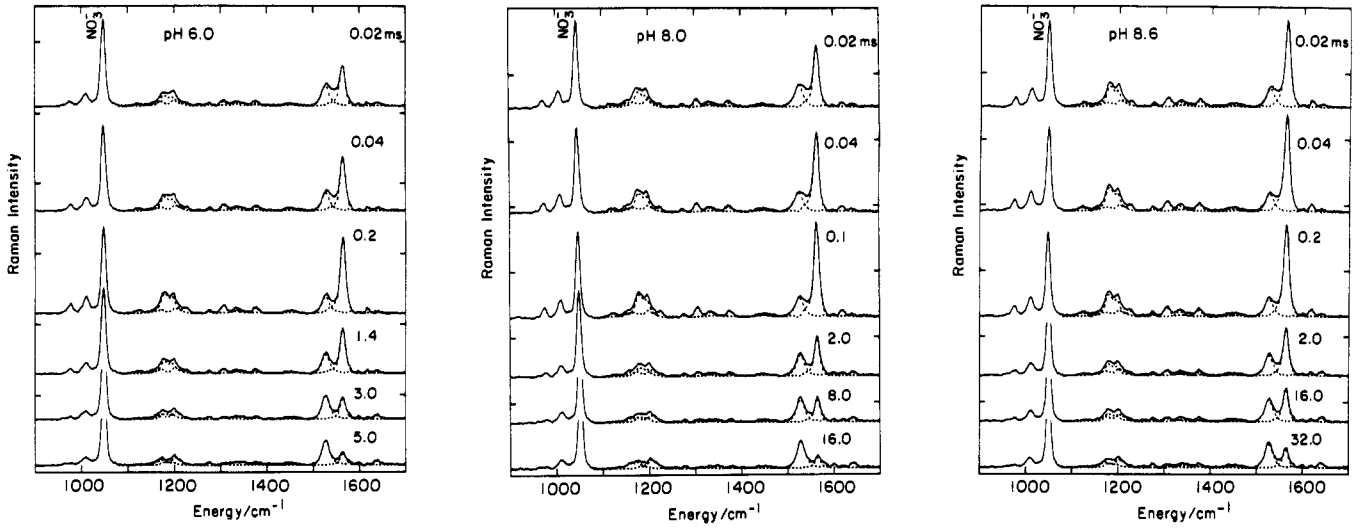

FIGURE 3: Kinetic pump + probe resonance Raman spectra of M_{412} at pH 6, 8, and 8.6 (probed at 457.9 nm). The dotted lines represent contributions from BR_{568} and M_{412}.

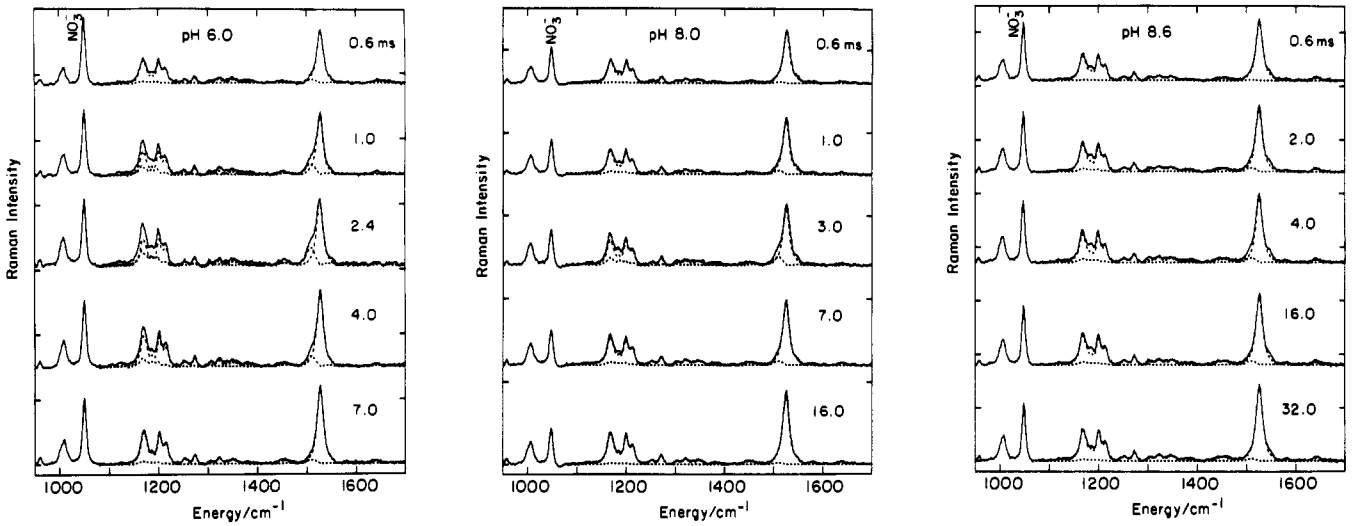

FIGURE 4: Kinetic pump + probe resonance Raman spectra of O_{640} at pH 6, 8, and 8.6 (probed at 752.4 nm). The dotted lines represent contributions from BR_{568} and O_{640}.

O_{640} basis spectra. The O_{640} amplitude gets smaller at high pH and decays more slowly.

The spectral contributions of the intermediates at each time were converted into absolute concentrations through the conservation of molecules least-squares refinement. This gave relative Raman cross section values (for the sum of all lines in the fitting region) of $\sigma_L/\sigma_{BR} = 1$ and $\sigma_N/\sigma_{BR} = 0.9$ at 501.7 nm, $\sigma_M/\sigma_{BR} = 4$ at 457.9 nm, and $\sigma_O/\sigma_{BR} = 6$ at 752.4 nm. By use of these values, the absolute concentration of each intermediate as well as the total concentration at each time point was determined. A complete list of the concentration of L_{550}, M_{412}, N_{550}, O_{640}, and BR_{568} as a function of time and pH is provided in the supplementary material, and these data are plotted in Figure 5. The total concentration is very close to 1 at all times and pH's with little systematic deviation. Although the conservation of molecules could be improved by allowing the relative cross sections to be pH-dependent, the improvement in the residuals was not sufficient to justify the additional parameters.

Kinetic Modeling. A series of kinetic schemes were examined to find the simplest one that accurately describes the data. The optimal rate constants for a given kinetic scheme were determined by the nonlinear least-squares procedure. The subscripts on the rate constants and their order denote the role of the constant. For example, k_{LM} is the forward rate constant for the L_{550} to M_{412} transition and k_{ML} is the corresponding reverse rate constant. *It is important to note that since we are fitting to absolute concentrations, our analysis determines the microscopic rate constants for the* **individual elementary steps** *of the photocycle reactions as opposed to apparent rate constants which simply describe the overall observed rate (and hence depend on a number of microscopic processes).*

Figure 6 shows the concentration of L_{550} as a function of time at pH 5. These data have been fit by a sequential scheme with (solid line) and without (dotted line) the $L_{550} \leftarrow M_{412}$ back-reaction. The biphasic L_{550} decay cannot be modeled well without the back-reaction. Including a back-reaction between L_{550} and M_{412} allows the biphasic L_{550} decay to be accurately described within the experimental error. Figure 7 presents the temporal profile of M_{412} at pH 8.6 which has been analyzed by using a sequential scheme with (solid line) and without (dotted line) the $M_{412} \leftarrow N_{550}$ back-reaction. Including the $M_{412} \leftarrow N_{550}$ back-reaction allows the biphasic decay of M_{412} to be modeled properly. Including the $N_{550} \leftarrow O_{640}$ and $O_{640} \leftarrow BR_{568}$ back-reactions does not improve the kinetic fits significantly. k_{BRO} and k_{ON} were both found to vary between ± 0.2 ms^{-1} depending on whether the initial estimate of k_{ON} was greater or less than 0.01 ms^{-1}. Thus, the

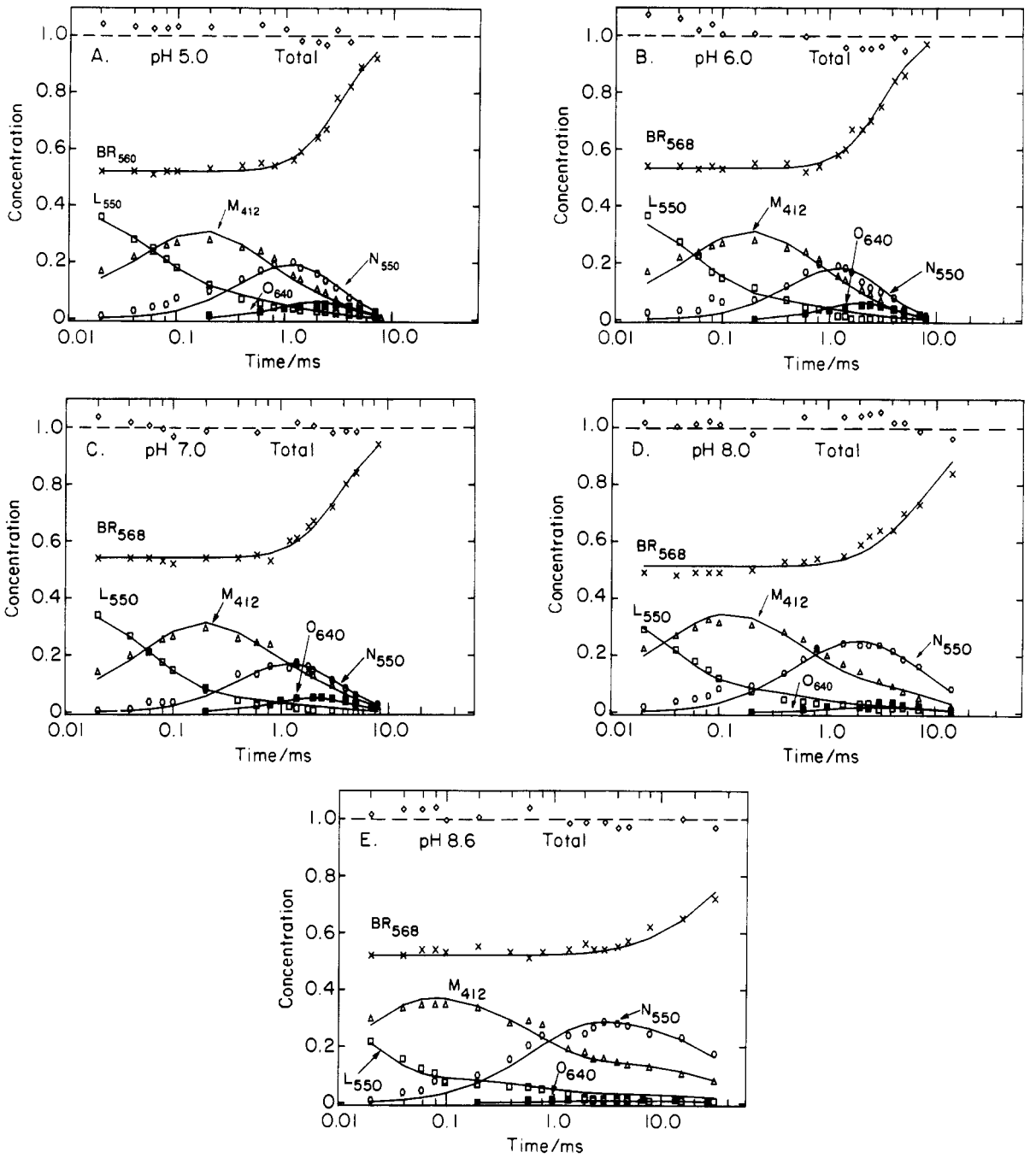

FIGURE 5: Concentration of L_{550}, M_{412}, N_{550}, O_{640}, and BR_{568} as a function of time at pH 5 (A), 6 (B), 7 (C), 8 (D), and 8.6 (E). The data points at the top show the total concentration of BR that results from the conservation of molecules refinement. The solid lines represent calculated concentrations for the best-fit kinetic scheme BR → L ↔ M ↔ N → O → BR using constants in Table I. The solvent conditions were 3 M KCl, 0.5 M nitrate, and 10 mM HEPES or borate (pH 8.6) at 30 °C. The measured concentrations are represented by the discrete data points with relative errors of ±10%.

Table I: Rate Constants for the Bacteriorhodopsin Photocycle[a]

pH	k_{LM}	k_{ML}	k_{MN}	k_{NM}	k_{NO}	k_{OBR}
5	12 ± 0.40	3.5 ± 0.30	1.6 ± 0.05	0.52 ± 0.05	0.56 ± 0.02	1.7 ± 0.16
6	13 ± 0.62	2.9 ± 0.4	1.5 ± 0.06	0.55 ± 0.07	0.60 ± 0.03	1.9 ± 0.24
7	14 ± 0.51	2.3 ± 0.31	1.3 ± 0.05	0.55 ± 0.05	0.54 ± 0.02	1.8 ± 0.20
8	21 ± 1.0	4.9 ± 0.53	1.4 ± 0.05	0.48 ± 0.04	0.15 ± 0.008	2.2 ± 0.53
8.6	40 ± 2.2	9.4 ± 0.81	1.2 ± 0.04	0.52 ± 0.03	0.03 ± 0.002	2.0 ± 1.1

[a] Rate constants are in ms^{-1} for the scheme: L ↔ M ↔ N → O → BR. The subscript on the constants denotes the kinetic process (e.g., k_{LM} is for $L_{550} \rightarrow M_{412}$ and k_{ML} is for $M_{412} \rightarrow L_{550}$). The solvent conditions were 3 M KCl, 0.5 M nitrate, and 10 mM HEPES or 10 mM borate (pH 8.6) at 30 °C. The standard deviations were extracted from the least-squares error matrix.

values of k_{BRO} and k_{ON} are indeterminate and were set equal to zero. *This analysis shows that the data are optimally modeled by the sequential scheme: $BR_{568} \rightarrow L_{550} \leftrightarrow M_{412} \leftrightarrow N_{550} \rightarrow O_{640} \rightarrow BR_{568}$.* The optimum rate constants at all pH's are listed in Table I, and the calculated concentrations at pH 5, 6, 7, 8, and 8.6 are given by the solid lines in Figure 5.

Figure 8 plots the optimum rate constants as a function of pH. Most of the rate constants are quite insensitive to pH. However, k_{LM}, k_{ML}, and k_{NO} change dramatically as the pH changes from 5 to 8.6. The pH dependence of k_{LM} and k_{ML}

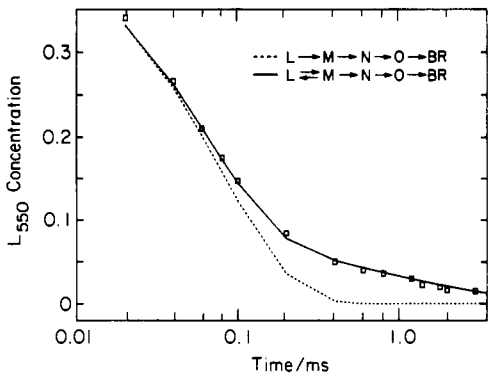

FIGURE 6: Analysis of the biphasic decay of L_{550} at pH 5. The dotted line presents the best-fit calculated concentration of L_{550} according to the scheme L → M → N → O → BR. The solid line presents the concentration of L_{550} calculated with the scheme L ↔ M → N → O → BR.

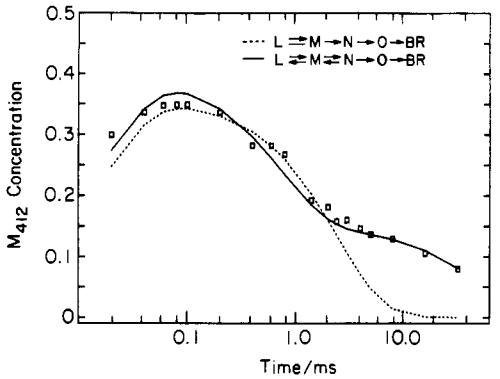

FIGURE 7: Analysis of the biphasic decay of M_{412} at pH 8.6. The dotted line presents the best-fit concentration of M_{412} calculated according to the kinetic scheme L ↔ M → N → O → BR. The solid line presents the concentration of M_{412} calculated with the scheme L ↔ M ↔ N → O → BR.

is consistent with the sigmoidal character observed by Rosenbach et al. (1982), with both rate constants rising sharply above pH 8. k_{NO} is independent of pH below 7, but it decreases with pH above 7 in agreement with Kouyama et al. (1988) and Otto et al. (1989).

Discussion

The goal of this study was to directly measure and model the kinetic behavior of the chemical species in the bacteriorhodopsin photocycle. The kinetics of L_{550}, M_{412}, N_{550}, O_{640}, and BR_{568} were measured from pH 5 to 8.6 by time-resolved Raman spectroscopy. After conversion to absolute concentrations by using conservation of molecules, these data were accurately modeled by a simple sequential scheme (L_{550} ↔ M_{412} ↔ N_{550} → O_{640} → BR_{568}) including back-reactions between L_{550} and M_{412} and between M_{412} and N_{550}. Although the residuals of the Raman kinetic profiles are not as low as those from time-resolved absorption measurements (Maurer et al., 1987; Xie et al., 1987), global modeling of the kinetic absorption data is severely hampered by the overlapping spectra of the intermediates (Hofrichter et al., 1989; Lozier et al., 1975; Zimanyi et al., 1989). Since the absorption basis spectra of the intermediates must be determined by the kinetic analysis, the spectra are generally dependent on the kinetic scheme used in the analysis. In contrast, the resonance Raman spectra exhibit a number of well-separated and distinctive vibrational lines, permitting a clear determination of the basis spectra and a clear separation of the kinetic profiles for each intermediate. The kinetic separation provided by the Raman spectra permits the generation of absolute concentrations which lead to an overdetermined kinetic analysis.

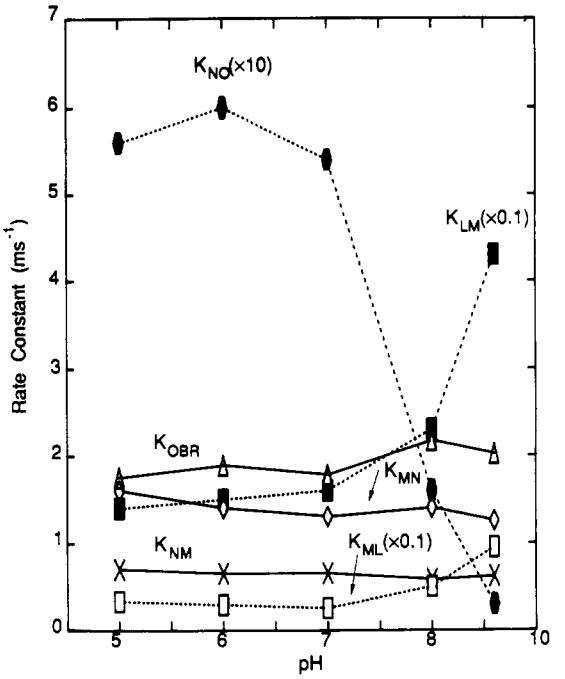

FIGURE 8: Best-fit rate constants for the bacteriorhodopsin photocycle versus pH using the kinetic scheme L ↔ M ↔ N → O → BR. The rate constants are indicated by the following symbols: k_{LM} (■), k_{ML} (□), k_{MN} (◇), k_{NM} (×), k_{NO} (●), and k_{OBR} (△).

The biphasic decay of L_{550} and M_{412} was one of the key features of the photocycle that we wanted to explain. We have shown here that finite rate constants for the L_{550} ← M_{412} and M_{412} ← N_{550} back-reactions are sufficient to accurately model the observed biphasic decay of L_{550} and M_{412} (Figures 6 and 7).[4] A sequential scheme with M_{412} ← N_{550} and N_{550} ← O_{640} back-reactions was also recently proposed on the basis of transient absorption studies (Chernavskii et al., 1989; Otto et al., 1989). Alternative kinetic schemes which employ two forms of L_{550} and M_{412} (Dancshazy et al., 1988; Diller & Stockburger, 1988; Hanamoto et al., 1984; Kouyama et al., 1988; Nakagawa et al., 1989) may also be consistent with the biphasic kinetics; however, until convincing evidence of *chemically* distinct forms has been presented, the presence of back-reactions must be the preferred explanation.

The kinetic resonance Raman spectra of L_{550} and N_{550} show that they are two different intermediates which appear sequentially in a single photocycle. Although L_{550} and N_{550} have the same nominal chromophore structure (Fodor et al., 1988a,b), the different frequencies and intensities of the methyl rock, C–C, and C=C stretch modes in Figure 1 show that these are chemically distinct intermediates. At neutral pH it is difficult to kinetically separate L_{550} and N_{550} unless a detailed analysis is performed as in Figure 5. At alkaline pH, the kinetics of L_{550} and N_{550} become resolved because L_{550} decays faster and N_{550} decays slower. The kinetic profiles and analysis at pH 8.0 and especially 8.6 (see Figure 5D,E) clearly show that N_{550} rises as M_{412} decays, demonstrating that N_{550} follows M_{412} in a sequential scheme. Since the same kinetic scheme accurately describes both the high-pH and neutral-pH data, this strongly argues that M_{412} decays into N_{550} under all the conditions studied here.

Diller and Stockburger (1988) have argued that L_{550} and N_{550} arise from two different photocycles because the *apparent*

[4] The principle of microscopic reversibility *requires* that every elementary step be reversible. Thus, if the inclusion of back-reactions in a kinetic scheme is sufficient to accurately describe the data, then this solution has no ad hoc assumptions.

rise time of N_{550} at pH 7.4 and 4.6 in 50 mM phosphate does not match the apparent decay time of M_{412}. Fodor et al. (1988a) showed that the fast decay time of M_{412} equals the rise time of N_{550} at pH 9.5 in high salt (3 M KCl). The apparent disagreement arises from the different conditions employed in these experiments. Using low-pH and low-salt conditions (see Figure 5A–C), it is not useful to compare the *apparent* rise of N_{550} to the *apparent* decay of M_{412} because there is insufficient kinetic separation of the various species. When the decay of N_{550} is rapid relative to its rise, the N_{550} concentration profile will tend to track that of M_{412}. One way to solve this problem is to choose alkaline pH and high-salt conditions where there is much better kinetic separation between L_{550}, M_{412}, and N_{550}. Alternatively, absolute concentrations can be analyzed to clarify the kinetic role of each intermediate as done here.

The pH dependence of the L ↔ M step provides important information about catalytic residues in the photocycle. k_{LM} and k_{ML} increase together while their ratio stays nearly constant as the pH increases from 5 to 8.6. This shows that alkaline pH acts to catalyze the L_{550} to M_{412} transition. Mass action arguments predict a slower $L_{550} \leftarrow M_{412}$ back-reaction at alkaline pH since the L_{550} to M_{412} transition involves Schiff base deprotonation. However, the fact that k_{LM} and k_{ML} increase together indicates that *alkaline pH simply catalyzes the L_{550} to M_{412} transition and that proton release from the protein is not a rate-determining step at the pH's studied here.* The presence of a catalytic tyrosine residue has been previously suggested on the basis of the pH dependence of the M_{412} rise kinetics observed in transient absorption studies (Hanamoto et al., 1984; Kalisky et al., 1981; Rosenbach et al., 1982). In this model, the two protonation states of the tyrosine alter the rate constants for the $L_{550} \leftrightarrow M_{412}$ transition. Near neutral pH, virtually all of the protein is in the protonated form and there is no sensitivity of the rate constants to pH. Thus, it is reasonable to think of the photocycle as arising from a single homogeneous pigment. At pH 8.6, the $L_{550} \leftrightarrow M_{412}$ rate constants are sensitive to pH, indicating a change in the relative amounts of the protonated and deprotonated forms of the protein. The chemical relaxation rate of tyrosine at pH 8.6 can be estimated to be ~40 ms (assuming diffusion-limited protonation); so, the tyrosine protonation state is effectively static for the majority of the photocycle. However, none of the rate constants for the steps following M_{412} exhibit a pH titration behavior similar to that seen for the $L_{550} \leftrightarrow M_{412}$ rate constants. Therefore, if the protonation state of a tyrosine does control the $L_{550} \leftrightarrow M_{412}$ kinetics, it does not affect the $M_{412} \leftrightarrow N_{550}$ or $O_{640} \rightarrow BR_{568}$ rates.

Proton Uptake during N_{550} Decay. The pH dependence of k_{NO} provides detailed information about the proton uptake process during proton pumping. Above pH 7, the N_{550} decay constant decreases with bulk pH, consistent with the work of Kouyama et al. (1988) and Otto et al. (1989) which indicate a linear relation with a slope of 1 from pH 8 to 12. However, at pH's ≤7, k_{NO} becomes pH independent. We conclude from the pH dependence of k_{NO} that two sequential elementary steps must take place between N_{550} and O_{640}: $N_{550} + H^+ \rightarrow N^+_{550} \rightarrow O_{640}$. Above pH 7, the protonation of a protein residue in the $N_{550} \rightarrow N^+_{550}$ step is rate-determining, whereas below pH 8 the cis-to-trans chromophore isomerization in the $N^+_{550} \rightarrow O_{640}$ step becomes rate determining. The protonation of the protein during $N_{550} \rightarrow N^+_{550}$ must be the proton taken up from the cytoplasm during proton pumping. This may account for the noticeable lag between the M_{412} fast decay kinetics and the rate of proton uptake (Kouyama et al., 1988; Lozier et al., 1976; Otto et al., 1989) and demonstrates that reprotonation of the Schiff base and proton uptake by the protein occur in two separate sequential steps. This is supported by recent mutagenesis studies on BR which indicate that Asp-96 serves as an internal proton donor to the Schiff base (Holz et al., 1989; Otto et al., 1989; Tittor et al., 1989).

A Model for Proton Pumping. In Figure 9 we present a molecular graphics model for each photocycle intermediate to illustrate a molecular mechanism of proton pumping. We assume the same folding pattern and secondary structure proposed by Huang et al. (1982) and the preferred helix assignments of Engelman et al. (1980). This is essentially identical with the structure recently presented by Leder et al. (1989) and Lin and Mathies (1989) and with the structure refined to the 3-D electron diffraction data on BR_{568} (Henderson et al., 1990). It is also similar to the model presented earlier by Braiman et al. (1988). The all-trans chromophore in BR_{568} is weakly hydrogen-bonded to Asp-212 (Lin & Mathies, 1989). It has also been suggested that the ionized Asp-212 and Asp-85 residues are stabilized electrostatically by the nearby Arg-82 (Braiman et al., 1988; Stern & Khorana, 1989), forming a complex counterion (De Groot et al., 1989).

Photoisomerization to produce K carries the Schiff base away from Asp-212 toward Asp-85. The Schiff base counterion is Asp-85 in K and L_{550}, consistent with observations that substitution of Asp-85 with asparagine eliminates proton-pumping activity (Mogi et al., 1988) and formation of M_{412} (Stern et al., 1989). During the $K \rightarrow L_{550}$ transition, the 13-cis chromophore conformationally relaxes as evidenced by the reduced HOOP intensity in the resonance Raman spectrum and forms a stronger hydrogen bond with Asp-85 (Fodor et al., 1988b).

In the $L_{550} \rightarrow M_{412}$ transition, the Schiff base proton is transferred to Asp-85. Protonation of Asp-85 initiates the release of a proton to the exterior (perhaps from Arg-82). The protonation of Asp-85 in M_{412} is clearly evident from the FTIR BR → M difference data (Braiman et al., 1988). However, the evidence for the protonation of Asp-212 in M_{412} is not as compelling and may also represent a change of environment around Asp-212. A unique aspect of our model is that Schiff base deprotonation is accompanied by a T → C protein conformational change which shifts the Schiff base away from Asp-85, causing the Schiff base lone pair to change orientation, thereby connecting it to the cytoplasm (Fodor et al., 1988a). The large frequency changes in amide I and II modes in the BR → M FTIR difference spectra provide support for a protein conformational change in M_{412} (Braiman et al., 1987). Neutron diffraction (Dencher et al., 1989) and light scattering studies (Drachev et al., 1989) also support conformational changes in M_{412}. The T → C transition is the molecular mechanism for the reprotonation switch, allowing the 13-cis chromophore to donate a proton to Asp-85 (during $L_{550} \leftrightarrow M_{412}$) and subsequently accept a proton from a cytoplasmic residue during M_{412} decay.

Reprotonation of the Schiff base and cytoplasmic proton uptake by the protein occur in two separate sequential steps which are driven by the net negative charge in the binding sites of M_{412} and N_{550}. During the $M_{412} \rightarrow N_{550}$ transition, Asp-96 donates a proton to the Schiff base via some intermediate group, which could be Thr-89 and/or H_2O as suggested by Tittor et al. (1989). The involvement of Asp-96 is based on the suggestion that Asp-96 deprotonates in N_{550} (Gerwert et al., 1989) and the observation that substitution of Asp-96 by asparagine dramatically slows down the M_{412} decay (Holz et al., 1989; Otto et al., 1989) and decreases proton pumping

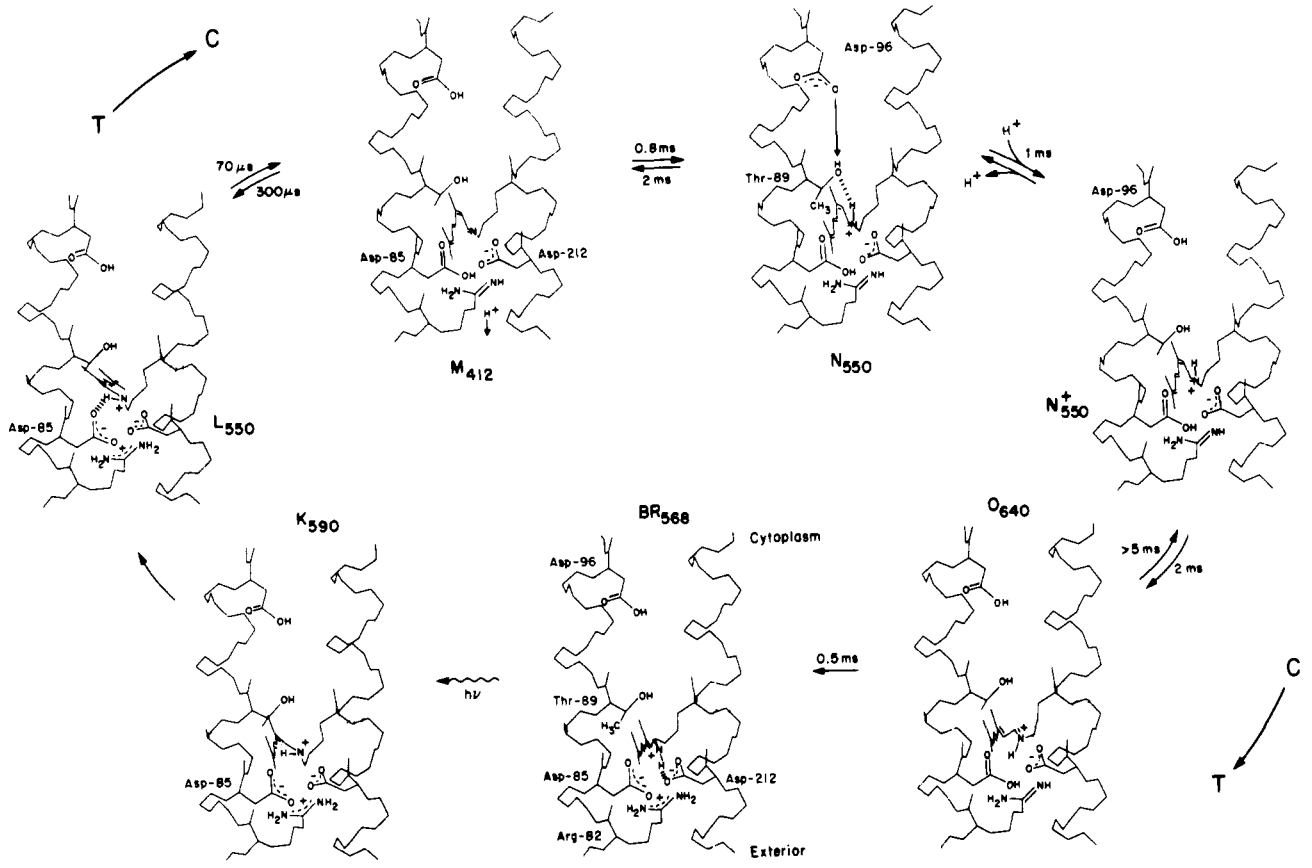

FIGURE 9: Molecular graphics representation for each of the bacteriorhodopsin photocycle intermediates. A side view of helices C and G is shown, highlighting residues Asp-85, Arg-82, Thr-89, Asp-96, Asp-212, and Lys-216 and their relation to the retinal chromophore. The indicated times are the reciprocal exponential rate constants for the elementary steps at neutral pH. A two-state protein conformational switch is used to control the connectivity of the Schiff base proton. In the T-state, the binding pocket sterically accommodates the 13-trans chromophore and the Schiff base group is connected to exterior residues. In the C-state, the pocket accommodates the 13-cis chromophore and the Schiff base is connected to cytoplasmic residues.

activity (Butt et al., 1989; Mogi et al., 1988). In the $N_{550} \rightarrow N^+_{550}$ transition, our kinetic studies indicate a protonation of the protein. Since Asp-96 reprotonates during proton uptake from the cytoplasm (Holz et al., 1989; Otto et al., 1989), it is reasonable to suggest that it protonates in the $N_{550} \rightarrow N^+_{550}$ transition.

The pump is reset by a reversal of the protein conformation from C → T which drives a concomitant cis → trans isomerization during $N^+_{550} \rightarrow O_{640}$. One of the key features of this model is that photoisomerization of the chromophore drives the protein from its "T" conformation to its "C" conformation, thereby storing energy in protein deformation. This stored energy is utilized in the N_{550} to O_{640} transition to drive the chromophore back to the all-trans configuration. The weak electrostatic interaction of the positive chromophore with the neutral Asp-85 accounts for the red-shifted λ_{max} in O_{640} consistent with the low-frequency C=N stretch (Smith et al., 1983). In the $O_{640} \rightarrow BR_{568}$ transition, the positive charge on the chromophore causes Asp-85 to transfer its proton to Arg-82 followed by conformational relaxation to bring the Schiff base group in contact with Asp-212. An intriguing prediction of this model is that if Arg-82 is removed, then proton release to the cell exterior from Asp-85 would be delayed until the $O_{640} \rightarrow BR_{568}$ transition, after proton uptake. This prediction has been dramatically confirmed by the recent work of Otto et al. (1990), lending support to this molecular mechanism.

Conclusions

The photocycle kinetics of bacteriorhodopsin can be accurately modeled by the scheme $BR_{568} \rightarrow L_{550} \leftrightarrow M_{412} \leftrightarrow N_{550} \rightarrow O_{640} \rightarrow BR_{568}$ from pH 5 to 8.6. This demonstrates that back-reactions are the most likely explanation for the biphasic kinetics of L_{550} and M_{412}. Furthermore, the structure of the chromophore in the N_{550} intermediate is independent of pH, and N_{550} is the direct decay product of M_{412} in a single photocycle. Finally, the pH dependence of k_{NO} indicates that proton uptake by the protein occurs during N_{550} decay.

Acknowledgments

We thank Stephen Fodor for assistance in setting up the time-resolved Raman experiments, W. Thomas Pollard for writing the least-squares kinetic refinement program, and Steve Lin for assistance in preparing the molecular graphics model. We also thank Walther Stoeckenius for his critical reading of the manuscript.

Supplementary Material Available

Figures 10–15, depicting the 502-, 458-, and 752-nm time-resolved resonance Raman data and basis spectral decomposition as a function of time at pH 5 and 7, and Table II, which presents a complete listing of the concentrations of BR_{568}, L_{550}, M_{412}, N_{550}, and O_{640} as a function of time at pH 5, 6, 7, 8, and 8.6 (7 pages). Ordering information is given on any current masthead page.

Registry No. Hydrogen, 12408-02-5.

References

Alshuth, T., & Stockburger, M. (1986) *Photochem. Photobiol. 43*, 55–66.

Ames, J. B., Fodor, S. P. A., Gebhard, R., Raap, J., van den Berg, E. M. M., Lugtenburg, J., & Mathies, R. A. (1989) *Biochemistry 28*, 3681–3687.
Argade, P. V., & Rothschild, K. J. (1983) *Biochemistry 22*, 3460–3466.
Aton, B., Doukas, A. G., Callender, R. H., Becher, B., & Ebrey, T. G. (1977) *Biochemistry 16*, 2995–2999.
Braiman, M., & Mathies, R. (1980) *Biochemistry 19*, 5421–5428.
Braiman, M. S., Ahl, P. L., & Rothschild, K. J. (1987) *Proc. Natl. Acad. Sci. U.S.A. 84*, 5221–5225.
Braiman, M. S., Mogi, T., Marti, T., Stern, L. J., Khorana, H. G., & Rothschild, K. J. (1988) *Biochemistry 27*, 8516–8520.
Butt, H. J., Fendler, K., Bamberg, E., Tittor, J., & Oesterhelt, D. (1989) *EMBO J. 8*, 1657–1663.
Cantor, C. R., & Schimmel, P. R. (1980) *Biophysical Chemistry*, W. H. Freeman and Co., San Francisco.
Chernavskii, D. S., Chizhov, I. V., Lozier, R. H., Murina, T. M., Prokhorov, A. M., & Zubov, B. V. (1989) *Photochem. Photobiol. 49*, 649–653.
Dancshazy, Zs., Govindjee, R., & Ebrey, T. G. (1988) *Proc. Natl. Acad. Sci. U.S.A. 85*, 6358–6361.
De Groot, H. J. M., Harbison, G. S., Herzfeld, J., & Griffin, R. G. (1989) *Biochemistry 28*, 3346–3353.
Dencher, N. A., Dresselhaus, D., Zaccai, G., & Buldt, G. (1989) *Proc. Natl. Acad. Sci. U.S.A. 86*, 7876–7879.
Deng, H., Pande, C., Callender, R. H., & Ebrey, T. G. (1985) *Photochem. Photobiol. 41*, 467–470.
Diller, R., & Stockburger, M. (1988) *Biochemistry 27*, 7641–7651.
Drachev, L. A., Kaulen, A. D., Skulachev, V. P., & Zorina, V. V. (1986) *FEBS Lett. 209*, 316–320.
Drachev, L. A., Kaulen, A. D., & Zorina, V. V. (1989) *FEBS Lett. 243*, 5–7.
Engelman, D. M., Henderson, R., McLachlan, A. D., & Wallace, B. A. (1980) *Proc. Natl. Acad. Sci. U.S.A. 77*, 2023–2027.
Fodor, S. P. A., Ames, J. B., Gebhard, R., van den Berg, E. M. M., Stoeckenius, W., Lugtenburg, J., & Mathies, R. A. (1988a) *Biochemistry 27*, 7097–7101.
Fodor, S. P. A., Pollard, W. T., Gebhard, R., van den Berg, E. M. M., Lugtenburg, J., & Mathies, R. A. (1988b) *Proc. Natl. Acad. Sci. U.S.A. 85*, 2156–2160.
Gerwert, K., Hess, B., Soppa, J., & Oesterhelt, D. (1989) *Proc. Natl. Acad. Sci. U.S.A. 86*, 4943–4947.
Hanamoto, J. H., Dupuis, P., & El-Sayed, M. A. (1984) *Proc. Natl. Acad. Sci. U.S.A. 81*, 7083–7087.
Henderson, R., Baldwin, J. M., Ceska, T. A., Zemlin, F., Beckmann, E., & Downing, K. H. (1990) *J. Mol. Biol. 213*, 899–929.
Hofrichter, J., Henry, E. R., & Lozier, R. H. (1989) *Biophys. J. 56*, 693–706.
Holz, M., Drachev, L. A., Mogi, T., Otto, H., Kaulen, A. D., Heyn, M. P., Skulachev, V. P., & Khorana, H. G. (1989) *Proc. Natl. Acad. Sci. U.S.A. 86*, 2167–2171.
Huang, K., Radhakrishnan, R., Bayley, H., & Khorana, H. G. (1982) *J. Biol. Chem. 257*, 13616–13623.
Kalisky, O., Ottolenghi, M., Honig, B., & Korenstein, R. (1981) *Biochemistry 20*, 649–655.
Khorana, H. G. (1988) *J. Biol. Chem. 263*, 7439–7442.
Kouyama, T., Nasuda-Kouyama, A., Ikegami, A., Mathew, M. K., & Stoeckenius, W. (1988) *Biochemistry 27*, 5855–5863.
Leder, R. O., Helgerson, S. L., & Thomas, D. D. (1989) *J. Mol. Biol. 209*, 683–701.
Lin, S. W., & Mathies, R. A. (1989) *Biophys. J. 56*, 653–660.
Lozier, R. H., Bogomolni, R. A., & Stoeckenius, W. (1975) *Biophys. J. 15*, 955–962.
Lozier, R., Niederberger, W., Bogomolni, R. A., Hwang, S.-B., & Stoeckenius, W. (1976) *Biochim. Biophys. Acta 440*, 545–556.
Mathies, R., Oseroff, A. R., & Stryer, L. (1976) *Proc. Natl. Acad. Sci. U.S.A. 73*, 1–5.
Mathies, R. A., Smith, S. O., & Palings, I. (1987) *Biological Applications of Raman Spectroscopy, Vol. 2: Resonance Raman Spectra of Polyenes and Aromatics* (Spiro, T. G., Ed.) pp 59–108, John Wiley and Sons, Inc., New York.
Mathies, R. A., Brito Cruz, C. H., Pollard, W. T., & Shank, C. V. (1988) *Science 240*, 777–779.
Maurer, R., Vogel, J., & Schneider, S. (1987) *Photochem. Photobiol. 46*, 247–253.
Mogi, T., Stern, L. J., Marti, T., Chao, B., & Khorana, H. G. (1988) *Proc. Natl. Acad. Sci. U.S.A. 85*, 4148–4152.
Nakagawa, M., Ogura, T., Maeda, A., & Kitagawa, T. (1989) *Biochemistry 28*, 1347–1352.
Otto, H., Marti, T., Holz, M., Mogi, T., Lindau, M., Khorana, H. G., & Heyn, M. P. (1989) *Proc. Natl. Acad. Sci. U.S.A. 86*, 9228–9232.
Otto, H., Marti, T., Holz, M., Mogi, T., Stern, L. J., Engel, F., Khorana, H. G., & Heyn, M. P. (1990) *Proc. Natl. Acad. Sci. U.S.A. 87*, 1018–1022.
Parodi, L. A., Lozier, R. H., Bhattacharjee, S. M., & Nagle, J. F. (1984) *Photochem. Photobiol. 40*, 501–512.
Rosenbach, V., Goldberg, R., Gilon, C., & Ottolenghi, M. (1982) *Photochem. Photobiol. 36*, 197–201.
Schneider, G., Diller, R., & Stockburger, M. (1989) *Chem. Phys. 131*, 17–29.
Schulten, K., & Tavan, P. (1978) *Nature 272*, 85–86.
Smith, S. O., Pardoen, J. A., Mulder, P. P. J., Curry, B., Lugtenburg, J., & Mathies, R. (1983) *Biochemistry 22*, 6141–6148.
Smith, S. O., Hornung, I., van der Steen, R., Pardoen, J. A., Braiman, M. S., Lugtenburg, J., & Mathies, R. A. (1986) *Proc. Natl. Acad. Sci. U.S.A. 83*, 967–971.
Stern, L. J., & Khorana, H. G. (1989) *J. Biol. Chem. 264*, 14202–14208.
Stern, L. J., Ahl, P. L., Marti, T., Mogi, T., Dunach, M., Berkowitz, S., Rothschild, K. J., & Khorana, H. G. (1989) *Biochemistry 28*, 10035–10042.
Stoeckenius, W., & Bogomolni, R. A. (1982) *Annu. Rev. Biochem. 51*, 587–616.
Terner, J., Hsieh, C.-L., & El-Sayed, M. A. (1979) *Biophys. J. 26*, 527–541.
Tittor, J., Soell, C., Oesterhelt, D., Butt, H.-J., & Bamberg, E. (1989) *EMBO J. 8*, 3477–3482.
Xie, A. H., Nagle, J. F., & Lozier, R. H. (1987) *Biophys. J. 51*, 627–635.
Zimanyi, L., Keszthelyi, L., & Lanyi, J. K. (1989) *Biochemistry 28*, 5165–5172.